Available online at www.sciencedirect.com

SciVerse ScienceDirect

Ceramics International 38 (2012) 2935–2941

CERAMICS INTERNATIONAL

www.elsevier.com/locate/ceramint

Effect of CaO addition on the structure and electrical conductivity of the pyrochlore-type $GdSmZr_2O_7$

Zhan-Guo Liu [a,b,c], Jia-Hu Ouyang [a,*], Ke-Ning Sun [b,c], Yu Zhou [a]

[a] School of Materials Science and Engineering, Harbin Institute of Technology, 92 West Da-Zhi Street, Harbin 150001, China
[b] Natural Science Research Center, Academy of Fundamental and Interdisciplinary Sciences, Harbin Institute of Technology, 2 Yi-Kuang Street, Harbin 150080, China
[c] Department of Applied Chemistry, Harbin Institute of Technology, 92 West Da-Zhi Street, Harbin 150001, China

Received 4 November 2011; received in revised form 25 November 2011; accepted 26 November 2011
Available online 4 December 2011

Abstract

Polycrystalline $GdSm_{1-x}Ca_xZr_2O_{7-x/2}$ ($0 \le x \le 0.20$) ceramics have been prepared by the solid-state reaction method. The effects of CaO addition on the microstructure and electrical properties of the pyrochlore-type $GdSmZr_2O_7$ ceramic were investigated. $GdSm_{1-x}Ca_xZr_2O_{7-x/2}$ ($x \le 0.05$) ceramics exhibit a pyrochlore-type structure; however, $GdSm_{1-x}Ca_xZr_2O_{7-x/2}$ ($0.10 \le x \le 0.20$) ceramics consist of the pyrochlore-type structure and a small amount of $CaZrO_3$. The total conductivity of $GdSm_{1-x}Ca_xZr_2O_{7-x/2}$ ceramics follows the Arrhenius relation, and gradually increases with increasing temperature from 723 to 1173 K. $GdSm_{1-x}Ca_xZr_2O_{7-x/2}$ ceramics are oxide-ion conductors in the oxygen partial pressure range of 1.0×10^{-4}–1.0 atm at each test temperature. The highest total conductivity is about 1.20×10^{-2} S cm^{-1} at 1173 K for the $GdSm_{0.9}Ca_{0.1}Zr_2O_{6.95}$ ceramic.

Keywords: C. Electrical conductivity; $GdSm_{1-x}Ca_xZr_2O_{7-x/2}$; Solid electrolyte; Structure; Impedance spectroscopy

1. Introduction

Solid oxide fuel cells (SOFCs) are one of the most attractive energy conversion systems owing to high power generation efficiency and very significant environmental advantages as compared with conventional power generation [1–4]. The durability of SOFCs is a very important factor in commercial SOFC systems. One of the crucial issues for the performance of SOFCs is the chemical stability of the cathode/electrolyte interface at elevated temperatures. Currently, SOFCs utilizes strontium-doped lanthanum manganite (LSM) as the cathode, 8 mol.% yttria stabilized zirconia (YSZ) as the electrolyte, and a Ni–YSZ cermet as the anode [5–7]. The reaction products of $La_2Zr_2O_7$ and $SrZrO_3$ would form at the interface of cathode/electrolyte at elevated temperatures [8–10]. These reaction products have a lower electrical conductivity than YSZ, which leads to the degradation of the performance of SOFCs. In recent years, the objective of SOFCs development is to reduce the operating temperature. For this purpose, the current emphasis mainly focuses on the search for solid oxide electrolytes with a higher electrical conductivity than YSZ [11–13].

The $Ln_2Zr_2O_7$-type (Ln = lanthanide) compounds exhibit a pyrochlore-type structure or a defect fluorite-type structure, and have a variety of interesting properties, including high melting point, high thermal stability, high thermal expansion coefficient, low thermal conductivity, and so on [14–17]. In the $Ln_2Zr_2O_7$-type structure, 7/8 anion sites are occupied by oxide-ions, while 1/8 anion sites are oxygen vacancy. $Ln_2Zr_2O_7$-type structure shows the well-known ability of the structure to accommodate oxygen nonstoichiometry [18]. The oxygen vacancy can be a source of excellent ionic conductivity allowing electrochemical applications such as solid oxide electrolytes or electrode materials. Van Dijk et al. found that the $Gd_2Zr_2O_7$ ceramic had a maximum in the electrical conductivity and a minimum in the activation energy at temperatures of 773 to 1023 K in $Gd_xZr_{1-x}O_{2-x/2}$ ($0.2 < x < 0.6$) ceramics prepared by a wet chemical method [19]. The electrical conductivity of SrO-doped $Gd_2Zr_2O_7$ is higher than that of undoped $Gd_2Zr_2O_7$ in the temperature range

* Corresponding author. Tel.: +86 451 86414291; fax: +86 451 86414291.
E-mail address: ouyangjh@hit.edu.cn (J.-H. Ouyang).

0272-8842/$36.00
doi:10.1016/j.ceramint.2011.11.070

of 773–973 K [20]. $(Gd_{1-x}Sm_x)_2Zr_2O_7$ ($0 \leq x \leq 1.0$) ceramics exhibited the highest electrical conductivity when the samarium dopant content was equal to 0.5 [21]. In the present study, the CaO-doped pyrochlore-type $GdSm_{1-x}Ca_xZr_2O_{7-x/2}$ ($x = 0$, 0.05, 0.10, 0.15, 0.20) were firstly prepared by pressureless-sintering method at 1973 K for 10 h in air. The objective of this work is to study the influence of CaO addition on the structure and electrical conductivity of the pyrochlore-type $GdSmZr_2O_7$ ceramic.

2. Experimental details

In this investigation, solid-state reaction was used to prepare CaO-doped $GdSm_{1-x}Ca_xZr_2O_{7-x/2}$ ($x = 0$, 0.05, 0.10, 0.15, 0.20) ceramics. Commercially available Gd_2O_3 (Rare-Chem Hi-Tech Co. Ltd., China; purity $\geq$ 99.99%), Sm_2O_3 (Rare-Chem Hi-Tech Co. Ltd., China; purity $\geq$ 99.99%), CaO (Tianjin Hengxing Chemical Preparation Co. Ltd., China; Analytical pure), and ZrO_2 (Dongguan SG Ceramics Technology Co. Ltd., China; purity $\geq$ 99.9%) were used as starting powders. All oxide powders were annealed at 1173 K for 2 h in air prior to weighing. The starting mixture with a nominal composition of $GdSm_{1-x}Ca_xZr_2O_{7-x/2}$ ($x = 0$, 0.05, 0.10, 0.15, 0.20) was mixed in analytically pure alcohol using zirconia balls for 24 h. The mixed powders were dried and ground in a mortar. The resultant powders were uniaxially compacted in a 15 mm die at 20 MPa, and then cold isostatically pressed at 200 MPa for 5 min to form pellets with a green density of about 45% of the theoretical density. The pressureless sintering process of green pellets was performed in a furnace at 1973 K for 10 h in air.

X-ray diffraction (XRD, Rigaku D/Max 2200VPC, Japan) with Cu Kα radiation was employed to identify the phase composition of the sintered samples at room temperature. XRD data were recorded in a 2θ range from 10° to 70° and in a continuous scan mode with a scanning rate of 4°/min. The bulk density of sintered samples was determined by the usual volume and weight measurement technique. The surface morphology was observed by a scanning electron microscope (SEM, FEI Quanta 200F, the Netherlands) coupled with energy-dispersive X-ray spectroscopy. A thin carbon coating was evaporated onto the surfaces of the samples for SEM observations.

Electrochemical impedance spectroscopy of the sintered samples was measured in air using an impedance/gain-phase analyzer (Solartron™ SI 1260, UK) with a frequency range of

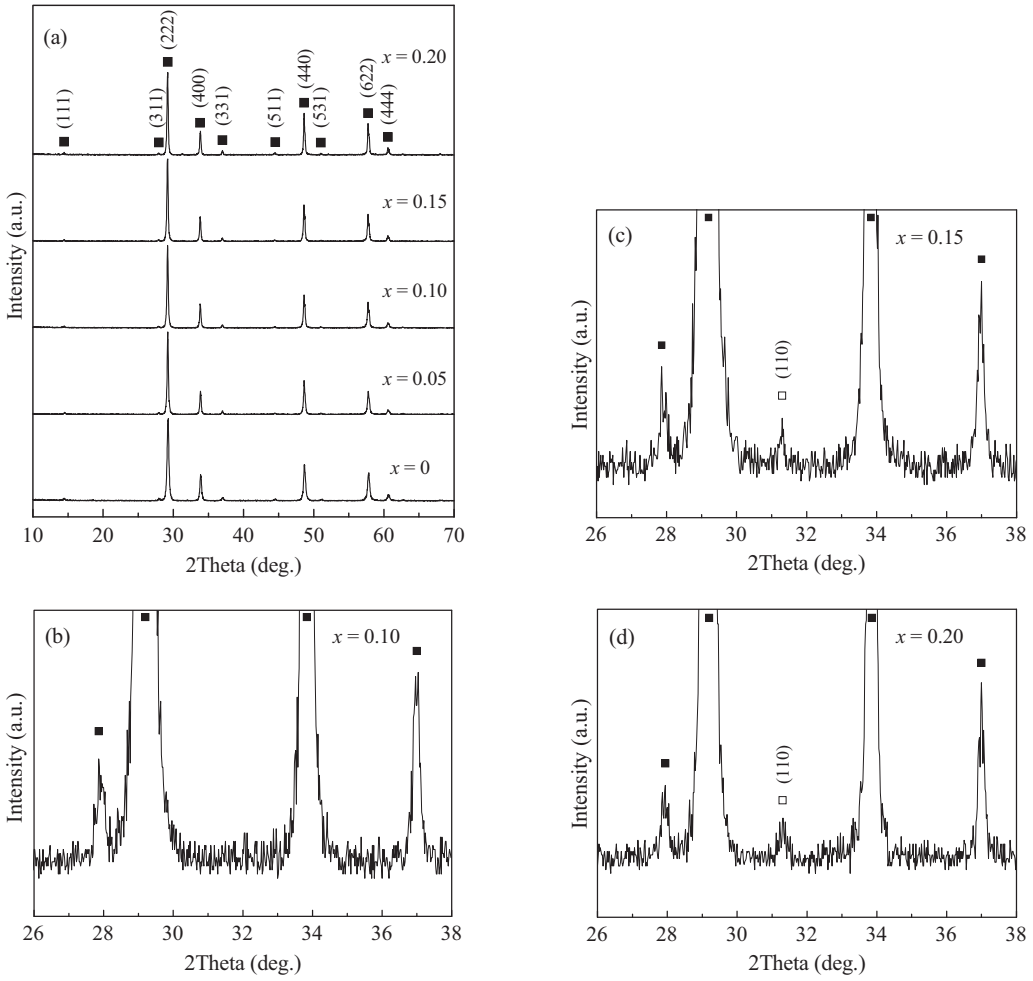

Fig. 1. XRD patterns of $GdSm_{1-x}Ca_xZr_2O_{7-x/2}$ ceramics sintered at 1973 K for 10 h in air: (a) 2θ range of 10°–70° and (b–d) 2θ range of 26°–38° for $x = 0.10$, 0.15 and 0.20, respectively (■, pyrochlore; □, $CaZrO_3$).

0.2 Hz–2 MHz and an AC amplitude of 20 mV. The well-polished samples with the dimensions of 8 mm in diameter and 1 mm in thickness were painted with platinum paste on both sides and baked at 1223 K for 2 h as electrodes. Platinum wires were attached to the surface of the samples for measurements. The impedance spectra were acquired during the heating process at temperatures of 723–1173 K with a dwell time of 30 min between consecutive measurements. The impedance dependence as a function of oxygen partial pressure $p(O_2)$ was obtained in a closed tube furnace cell. The oxygen partial

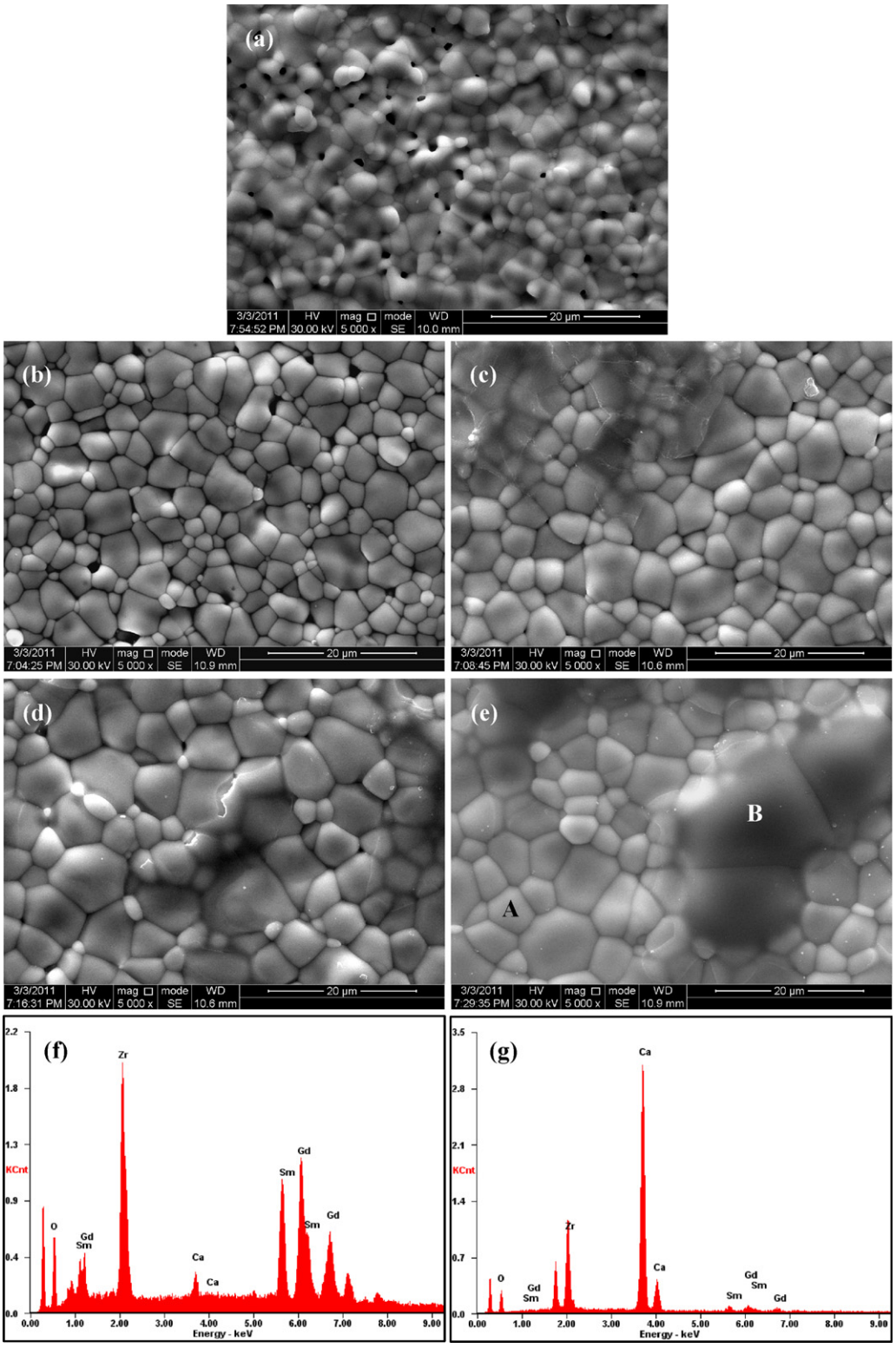

Fig. 2. Microstructures of as-sintered $GdSm_{1-x}Ca_xZr_2O_{7-x/2}$ ceramics: (a) $x = 0$, (b) $x = 0.05$, (c) $x = 0.10$, (d) $x = 0.15$, (e) $x = 0.20$, (f) and (g) EDS spectra at the locations of A and B in (e), respectively.

pressure ranged from about 1.0×10^{-4}–1.0 atm, and was monitored by an YSZ sensor. The process involved flushing the system with a N_2–O_2 gas mixture. Zview 3.1c software was used to analyze all impedance data.

3. Results and discussion

XRD patterns of $GdSm_{1-x}Ca_xZr_2O_{7-x/2}$ ceramics are shown in Fig. 1. X-ray diffraction spectra from both pure $GdSmZr_2O_7$ and CaO-doped $GdSmZr_2O_7$ ceramics show the cubic pyrochlore-type structure and confirm the presence of the $CaZrO_3$ by one small but distinct peak for $GdSm_{1-x}Ca_xZr_2O_{7-x/2}$ ($x = 0.15$, 0.20) ceramics, which is the most intense peak of $CaZrO_3$. Typical surface micrographs of as-sintered $GdSm_{1-x}Ca_xZr_2O_{7-x/2}$ ceramics are presented in Fig. 2. It can be seen from SEM images that $GdSm_{1-x}Ca_xZr_2O_{7-x/2}$ ceramics have a very high relative density except for $GdSmZr_2O_7$. The average grain size of the CaO-doped samples is obviously larger than that of un-doped samples, and the grain boundaries are very clean. From Fig. 2(c–e), the dark second phase can be clearly observed as contrasted with the results in Fig. 2(a–b). However, XRD patterns of the $GdSm_{0.9}Ca_{0.1}Zr_2O_{6.95}$ sample do not identify the existence of the second phase, which indicates that the amount of the second phase $CaZrO_3$ of the $GdSm_{0.9}Ca_{0.1}Zr_2O_{6.95}$ sample is low and is not able to be identified by XRD. The EDS spectra obtained at different positions of A and B in Fig. 2(f) confirm the presence of the pyrochlore-type phase (position A) and $CaZrO_3$ phase (position B), which is consistent with above XRD results. The relative density of the $GdSmZr_2O_7$ ceramic is 96.0%, and CaO-doped $GdSmZr_2O_7$ samples have a higher relative density than $GdSmZr_2O_7$, which is consistent with SEM observations. It indicates that the addition of calcia can promote the sintering densification behavior.

Fig. 3 shows a series of impedance plots and corresponding equivalent circuit model of $GdSm_{1-x}Ca_xZr_2O_{7-x/2}$ ceramics at 723 K. Three separate regions can be distinguished in the measured frequency range: the high frequency range represents the grain response (G), the intermediate frequency range is attributed to the grain boundary response (GB), and the low frequency range corresponds to the electrode contributions (E). The impedance plots were fitted using equivalent circuits consisting of a serial association of (*RC*) elements ascribed to electrolyte or electrode processes [22–24], where *R* is a resistance and *CPE* is a constant phase element in parallel, as shown in Fig. 3(f). From fitted results, the capacitance associated with the grain impedance was found to be in the order of pF, the capacitance for the grain boundary impedance is determined to be in the order of nF. These values are similar to the capacitance for grain and grain boundary impedance for

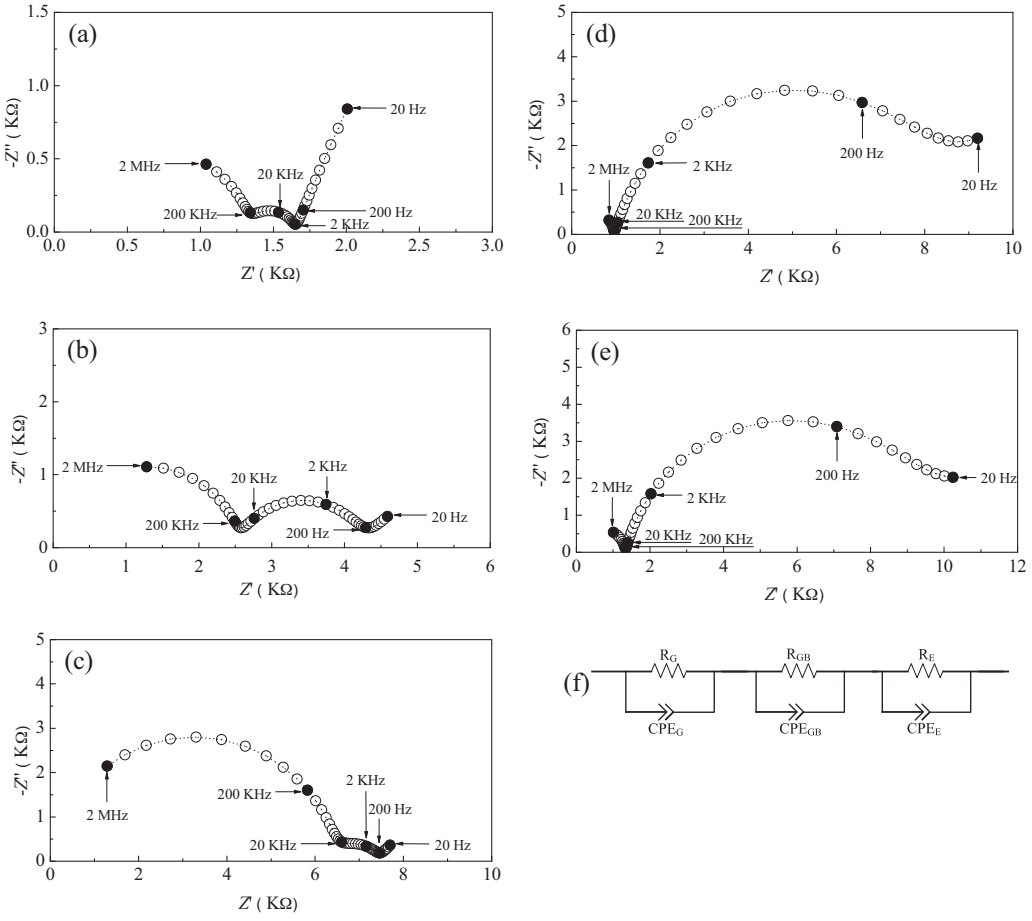

Fig. 3. Impedance spectra and schematic equivalent electrical circuit plots of $GdSm_{1-x}Ca_xZr_2O_{7-x/2}$ ceramics at 723 K in air: (a) $x = 0$, (b) $x = 0.05$, (c) $x = 0.10$, (d) $x = 0.15$, (e) $x = 0.20$ and (f) equivalent electrical circuit.

other ionic conductors [25], respectively. The total resistance (R_T) of $GdSm_{1-x}Ca_xZr_2O_{7-x/2}$ ceramics is given by

$$R_T = R_G + R_{GB} \quad (1)$$

where R_G and R_{GB} represent the grain resistance and grain boundary resistance, respectively. Both R_G and R_{GB} can be obtained by fitting the impedance plots. The total conductivity of $GdSm_{1-x}Ca_xZr_2O_{7-x/2}$ ceramics at different temperatures can be obtained using the following equation,

$$\sigma = \frac{L}{S \cdot R_T} \quad (2)$$

where L and S denote the thickness of the sample and the electrode area of the sample surface, respectively.

The temperature dependence of the total conductivity can be described by the Arrhenius equation with the following expression,

$$\sigma \cdot T = \sigma_0 \exp\left(\frac{-E}{k_B T}\right) \quad (3)$$

where σ, T, σ_0, E and k_B are the total conductivity, absolute temperature, pre-exponential factor, activation energy and Boltzmann's constant, respectively. Fig. 4 depicts Arrhenius plots of the total conductivity for $GdSm_{1-x}Ca_xZr_2O_{7-x/2}$ ceramics. It is evident that the total conductivity of $GdSm_{1-x}Ca_xZr_2O_{7-x/2}$ ceramics gradually increases with increasing temperature from 723 to 1173 K, respectively. The total conductivity of $GdSm_{1-x}Ca_xZr_2O_{7-x/2}$ ceramics follows the linear behavior with a typical correlation coefficient range of 0.9998–0.9999, which indicates that the ionic diffusion process is thermally activated. The activation energy and pre-exponential factor for the total conductivity for $GdSm_{1-x}Ca_xZr_2O_{7-x/2}$ ceramics are calculated from the slope and the intercept of the Arrhenius plots, respectively. The activation energy and pre-exponential factor are shown in Fig. 5. The activation energy and pre-exponential factor for the total conductivity of $GdSm_{1-x}Ca_xZr_2O_{7-x/2}$ ceramics obviously increase with increasing CaO content from $x = 0$ to $x = 0.10$, and slightly varies with further increase CaO content from $x = 0.10$ to $x = 0.20$.

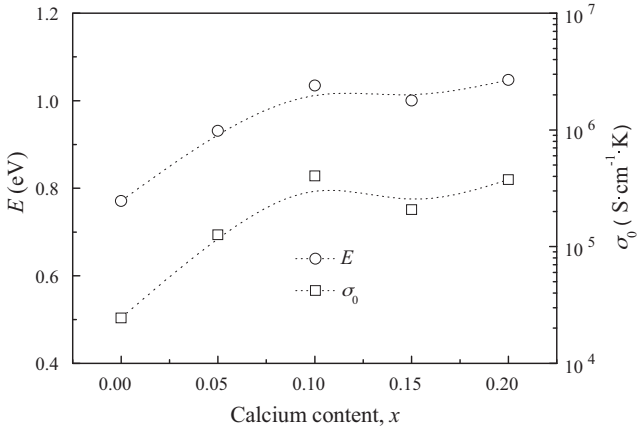

Fig. 5. Activation energy and pre-exponential factor for the total conductivity of $GdSm_{1-x}Ca_xZr_2O_{7-x/2}$ ceramics.

Fig. 6 displays the compositional dependence of the total conductivity of $GdSm_{1-x}Ca_xZr_2O_{7-x/2}$ ceramics as a function of CaO content at different temperatures. At temperatures of 723–973 K, the total conductivity of $GdSm_{1-x}Ca_xZr_2O_{7-x/2}$ ceramics slightly decreases with increasing CaO content at identical temperature levels. However, the total conductivity of $GdSm_{1-x}Ca_xZr_2O_{7-x/2}$ ceramics slightly increases with increasing CaO content from $x = 0$ to $x = 0.10$ in the temperature range of 1023–1173 K, and reach the maximum value of the total conductivity when the CaO content equals 0.10. The $GdSm_{0.9}Ca_{0.1}Zr_2O_{6.95}$ ceramic has the maximum value of the total conductivity, about 1.20×10^{-2} S cm^{-1} at 1173 K. In this work, the oxygen partial pressure $p(O_2)$ dependence of the total conductivity for $GdSm_{1-x}Ca_xZr_2O_{7-x/2}$ ceramics was also measured in order to clarify the conduction carrier. The total conductivity of $GdSm_{1-x}Ca_xZr_2O_{7-x/2}$ ceramics ($x = 0$, 0.10, 0.20) as a function of oxygen partial pressure at different temperatures is shown in Fig. 7. The total

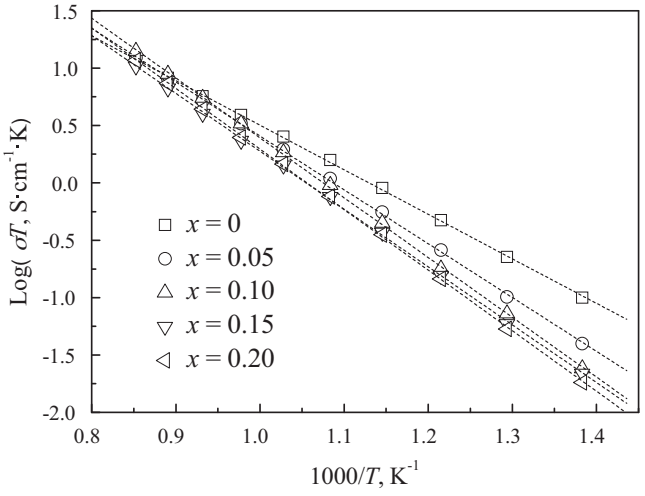

Fig. 4. Arrhenius plots of the total conductivity of $GdSm_{1-x}Ca_xZr_2O_{7-x/2}$ ceramics.

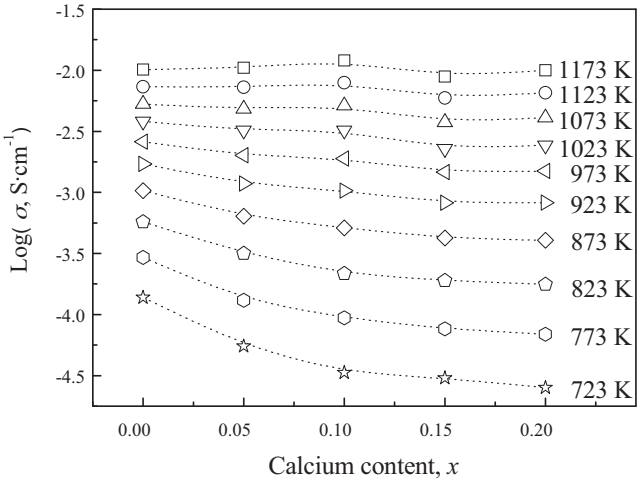

Fig. 6. Compositional dependence of the total conductivity of $GdSm_{1-x}Ca_xZr_2O_{7-x/2}$ ceramics as a function of CaO content.

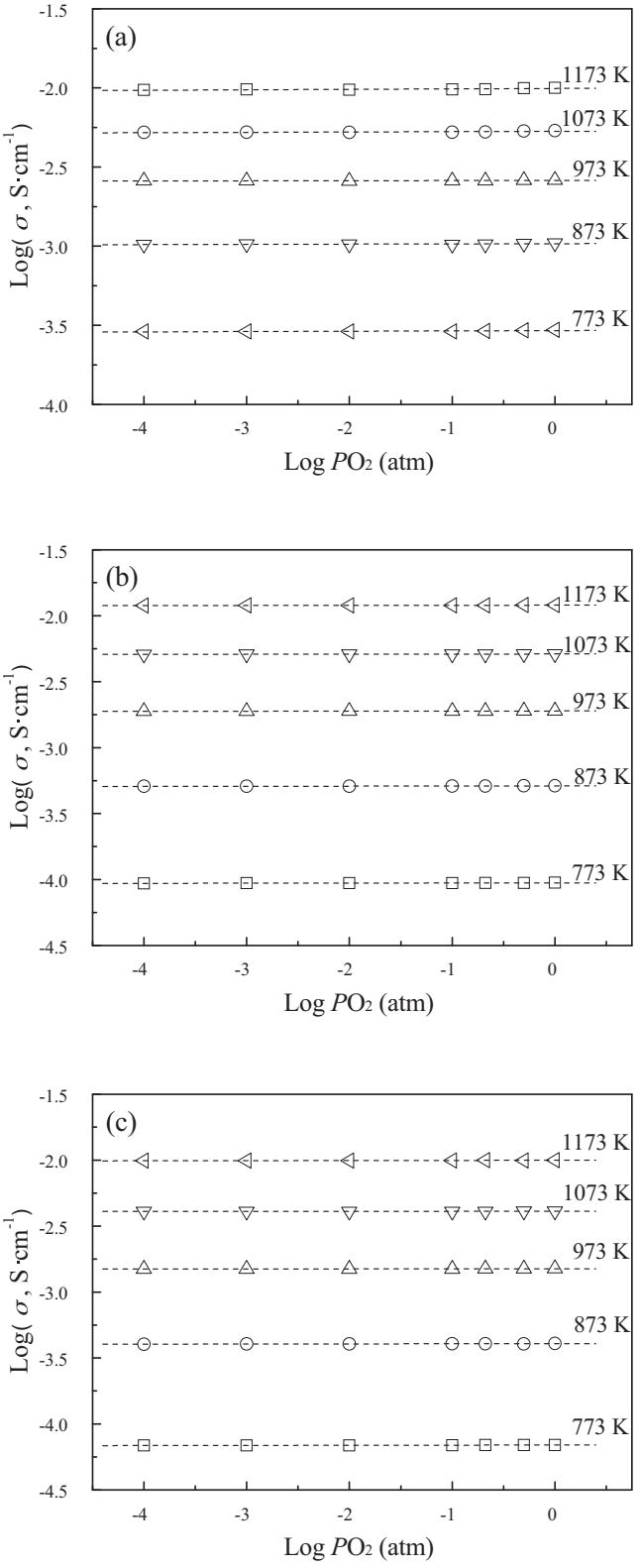

Fig. 7. Oxygen partial pressure dependence of the total conductivity of $GdSm_{1-x}Ca_xZr_2O_{7-x/2}$ ceramics: (a) $x = 0$, (b) $x = 0.10$, and (c) $x = 0.20$.

conductivity of $GdSm_{1-x}Ca_xZr_2O_{7-x/2}$ ceramics is almost independent of oxygen partial pressure from 1.0×10^{-4} to 1.0 atm at each test temperature, which confirms that the conduction is purely ionic with negligible electronic conduction [26]. From Fig. 6, the total conductivity of $GdSm_{1-x}Ca_xZr_2O_{7-x/2}$ ceramics is slightly lower than that of widely investigated solid electrolytes such as YSZ, $Sc_xZr_{1-x}O_{2-x/2}$ ($x = 0.08$–0.11), $Gd_{0.1}Ce_{0.9}O_{1.9}$ or $La_{0.8}Sr_{0.2}Ga_{0.8}Mg_{0.2}O_3$ [27], the most likely applications of $GdSm_{1-x}Ca_xZr_2O_{7-x/2}$ ceramics in SOFCs are high-temperature solid electrolytes, or thick-film electrolytes, or as protective layers applied onto CeO_2- or $LaGaO_3$-based electrolytes [28].

4. Conclusions

$GdSm_{1-x}Ca_xZr_2O_{7-x/2}$ ($x = 0$, 0.05) ceramics have a single phase of pyrochlore-type structure, and $GdSm_{1-x}Ca_xZr_2O_{7-x/2}$ ($x = 0.10$, 0.15, 0.20) ceramics are composed of pyrochlore phase and a small amount of $CaZrO_3$. The relative density of $GdSm_{1-x}Ca_xZr_2O_{7-x/2}$ ceramics is over 96.0%. The total conductivity of $GdSm_{1-x}Ca_xZr_2O_{7-x/2}$ ceramics follows the Arrhenius relation, and gradually increases with increasing temperature from 723 to 1173 K. $GdSm_{1-x}Ca_xZr_2O_{7-x/2}$ ceramics are oxide-ion conductors in the oxygen partial pressure range of 1.0×10^{-4}–1.0 atm at each test temperature. In the present work, the highest total conductivity is about 1.20×10^{-2} S cm^{-1} at 1173 K for the $GdSm_{0.9}Ca_{0.1}Zr_2O_{6.95}$ ceramic.

Acknowledgements

This work was financially supported by the National Natural Science Foundation of China (NSFC, Grant Nos. 50972030 and 51021002), and the Fundamental Research Funds for the Central Universities (Grant Nos. HIT.BRET1.2010006 and HIT.NSRIF.201132), and the China Postdoctoral Science Foundation funded project (CPSF-Nos. 20100471029 and 201104419).

References

[1] R.M. Ormerod, Solid oxide fuel cells, Chem. Soc. Rev. 32 (2003) 17–28.
[2] K. Kendall, Progress in solid oxide fuel cell materials, Int. Mater. Rev. 50 (2005) 257–264.
[3] H. Yokokawa, N. Sakai, T. Horita, K. Yamaji, M.E. Brito, Electrolytes for solid-oxide fuel cells, MRS Bull. 30 (2005) 591–595.
[4] M.C. Tucker, Progress in metal-supported solid oxide fuel cells: a review, J. Power Sources 195 (2010) 4570–4582.
[5] Y.S. Yoon, J.M. Im, D.W. Shin, Microstructure and electrical conductivity of NiO–YSZ nano-powder synthesized by aerosol flame deposition, Ceram. Int. 34 (2008) 873–876.
[6] T. Jardiel, B. Levenfeld, R. Jimenez, A. Varez, Fabrication of 8-YSZ thin-wall tubes by powder extrusion moulding for SOFC electrolytes, Ceram. Int. 35 (2009) 2329–2335.
[7] L.P. Sun, Q. Li, L.H. Huo, H. Zhao, G.Y. Zhang, N. Lin, J.P. Viricelle, C. Pijolat, Synthesis and performance of $Sr_{1.5}La_xMnO_4$ as cathode materials for intermediate temperature solid oxide fuel cell, J. Power Sources 196 (2011) 5835–5839.
[8] H.-C. Yu, K.-Z. Fung, Reaction between strontium-doped lanthanum cuprate and yittria-stabilized zirconia, J. Am. Ceram. Soc. 89 (2006) 2881–2886.
[9] C.A. Cortés-Escobedo, J. Muñoz-Saldaña, A.M. Bolarín-Miró, F.S. Jesús, Determination of strontium and lanthanum zirconates in YPSZ–LSM mixtures for SOFC, J. Power Sources 180 (2008) 209–214.

[10] M. Chen, Y.-L. Liu, A. Hagen, P.V. Hendriksen, F.W. Poulsen, LSM–YSZ reactions in different atmospheres, Fuel Cells 9 (2009) 833–840.
[11] S. Wang, F. Zhao, L. Zhang, K. Brinkman, F. Chen, Stability and electrical property of $Ba_{1-x}Sr_xCe_{0.8}Y_{0.2}O_{3-\delta}$ high temperature proton conductor, J. Alloys Compd. 506 (2010) 263–267.
[12] S.H. Jo, P. Muralidharan, D.K. Kim, Raman and ^{29}Si NMR spectroscopic characterization of lanthanum silicate electrolytes: emphasis on sintering temperature to enhance the oxide-ion conductivity, Electrochim. Acta 54 (2009) 7495–7501.
[13] Z.-G. Liu, J.-H. Ouyang, Y. Zhou, X.-L. Xia, Electrical conductivity of samarium–ytterbium zirconate ceramics, Electrochim. Acta 54 (2009) 3968–3971.
[14] M.A. Subramanian, G. Aravamudan, G.V. Subba Rao, Oxide pyrochlores—a review, Prog. Solid State Chem. 15 (1983) 55–143.
[15] Z.-G. Liu, J.-H. Ouyang, Y. Zhou, Preparation and thermophysical properties of $(Nd_xGd_{1-x})_2Zr_2O_7$ ceramics, J. Mater. Sci. 43 (2008) 3596–3603.
[16] Z.-G. Liu, J.-H. Ouyang, Y. Zhou, X.-L. Xia, Electrical conductivity and thermal expansion of neodymium–ytterbium zirconate ceramics, J. Power Sources 195 (2010) 3261–3265.
[17] Z. Xu, S. He, L. He, R. Mu, G. Huang, X. Cao, Novel thermal barrier coatings based on $La_2(Zr_{0.7}Ce_{0.3})_2O_7$–8YSZ double-ceramic-layer systems deposited by electron beam physical vapor deposition, J. Alloys Compd. 509 (2011) 4273–4283.
[18] C.R. Stanek, L. Minervini, R.W. Grimes, Nonstoichiometry in $A_2B_2O_7$ pyrochlores, J. Am. Ceram. Soc. 85 (2002) 2792–2798.
[19] T. van Dijk, K.J. de Vries, A.J. Burggraaf, Electrical conductivity of fluorite and pyrochlore $Ln_xZr_{1-x}O_{2-x/2}$ (Ln = Gd, Nd) solid solutions, Phys. Status Solidi A 58 (1980) 115–125.
[20] K.V. Govindan Kutty, C.K. Mathews, T.N. Rao, U.V. Varadaraju, Oxide ion conductivity in some substituted rare earth pyrozirconates, Solid State Ionics 80 (1995) 99–110.
[21] Z.-G. Liu, J.-H. Ouyang, Y. Zhou, X.-L. Xia, Effect of Sm substitution for Gd on the electrical conductivity of fluorite-type $Gd_2Zr_2O_7$, J. Power Sources 185 (2008) 876–880.
[22] Q.-A. Huang, R. Hui, B.W. Wang, J.J. Zhang, A review of AC impedance modeling and validation in SOFC diagnosis, Electrochim. Acta 52 (2007) 8144–8164.
[23] B. Rangarajan, S.S.N. Bharadwaja, E. Furman, T. Shrout, M. Lanagan, Impedance spectroscopy studies of fresnoites in $BaO–TiO_2–SiO_2$ system, J. Am. Ceram. Soc. 93 (2010) 522–530.
[24] T.P. Holme, R. Pornprasertsuk, F.B. Prinz, Interpretation of low temperature solid oxide fuel cell electrochemical impedance spectra, J. Electrochem. Soc. 157 (2010) B64–B70.
[25] Q. Li, V. Thangadurai, Synthesis, structure and electrical properties of Mo-doped CeO_2-materials for SOFCs, Fuel Cells 9 (2009) 684–698.
[26] J.B. Goodenough, Oxide-ion electrolytes, Annu. Rev. Mater. Res. 33 (2003) 91–128.
[27] J.W. Fergus, Electrolytes for solid oxide fuel cells, J. Power Sources 162 (2006) 30–40.
[28] V.V. Kharton, F.M.B. Marques, A. Atkinson, Transport properties of solid oxide electrolyte ceramics: a brief review, Solid State Ionics 174 (2004) 135–149.